Supplement of Earth Syst. Sci. Data, 18, 1103–1129, 2026
https://doi.org/10.5194/essd-18-1103-2026-supplement

Open Access Earth System Science Data

Supplement of

1 km annual forest cover and plant functional type dataset for China from 1981 to 2023

Bo Liu et al.

Correspondence to: Boyan Li (byli@snnu.edu.cn) and Qi Feng (qifeng@lzb.ac.cn)

Supplementary Figures S1 – S14

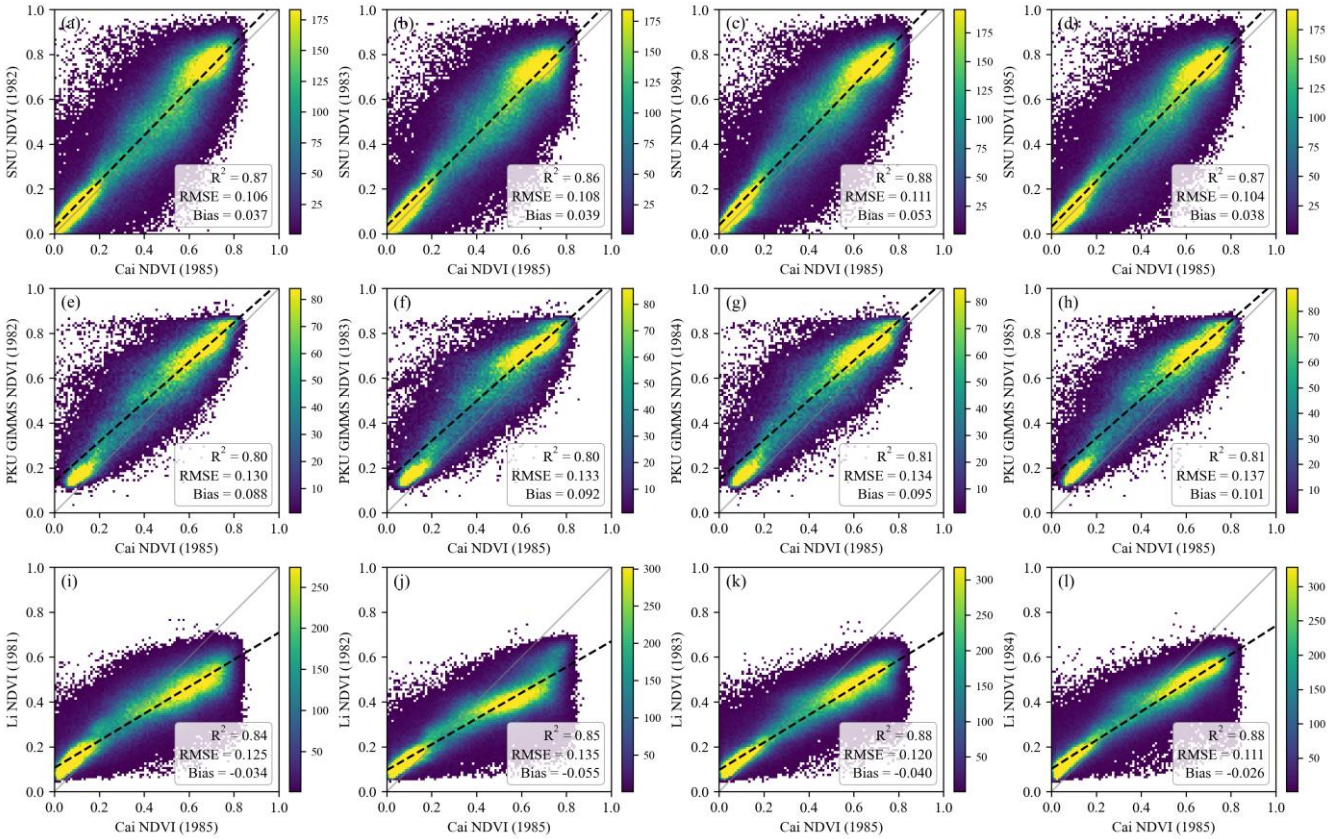

Figure S1. Pixel wise correlation analysis validating the representativeness of the 1985 NDVI dataset for the early 1980s. The scatter plots compare the growing season median NDVI from Cai et al. (2025) (1985 baseline, x-axis) against concurrent and preceding annual data from three independent long-term products (y-axis): **(a–d)** SNU NDVI (1982–1985), **(e–h)** PKU GIMMS NDVI (1982–1985), and **(i–l)** Li NDVI (1981–1984). The color scale represents point density. The solid grey line indicates the 1:1 line, and the black dashed line represents the linear regression fit. Statistical metrics (R^2, RMSE, and Bias) are provided in each panel.

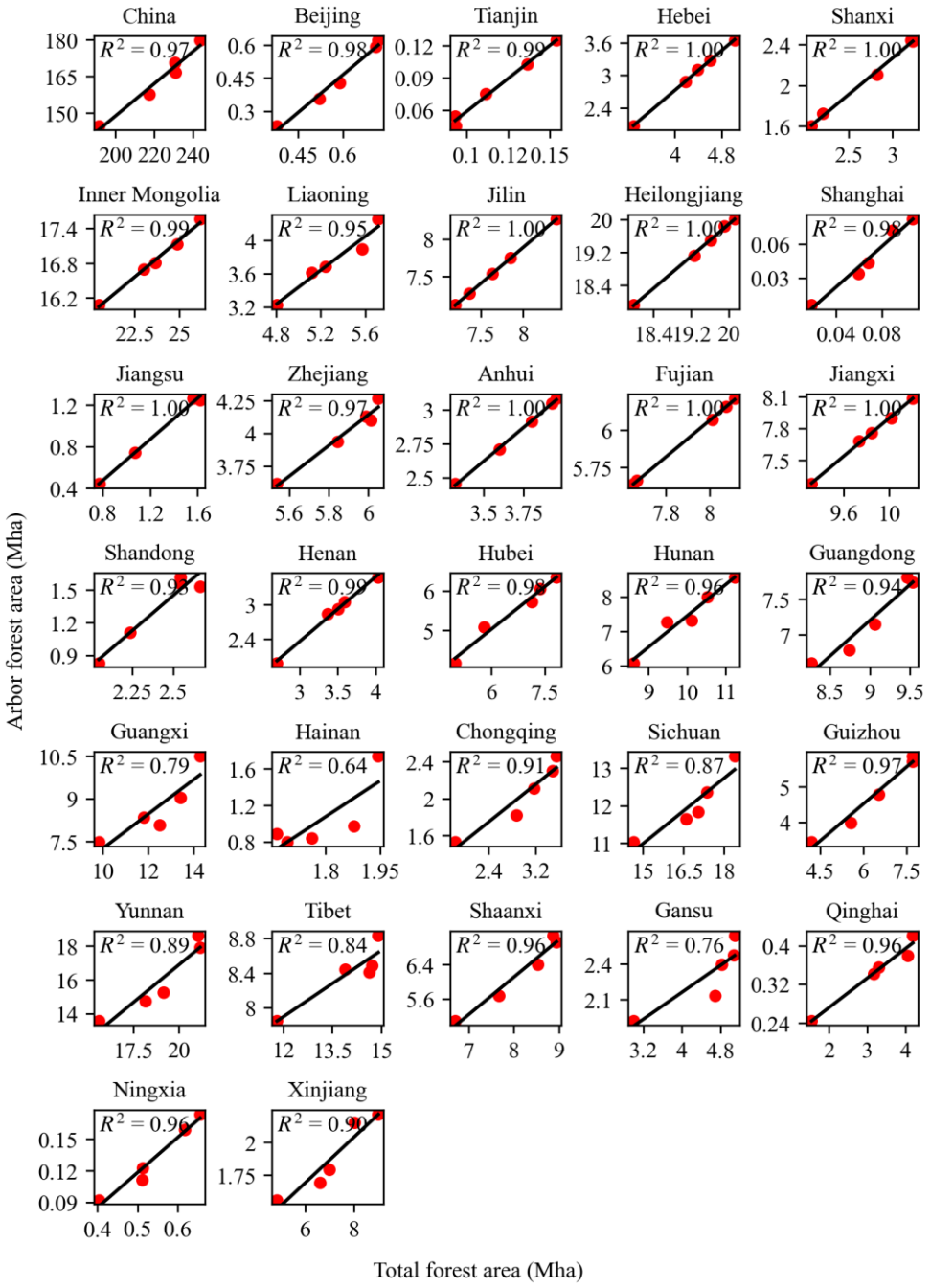

Figure S2. Extrapolation of arbor forest area for each province in China. Note: national forest inventories (NFI) statistics were unavailable for Hong Kong, Macau, and Taiwan (post-2013). We did not reconstruct these areas as they are not included in China's major afforestation programs.

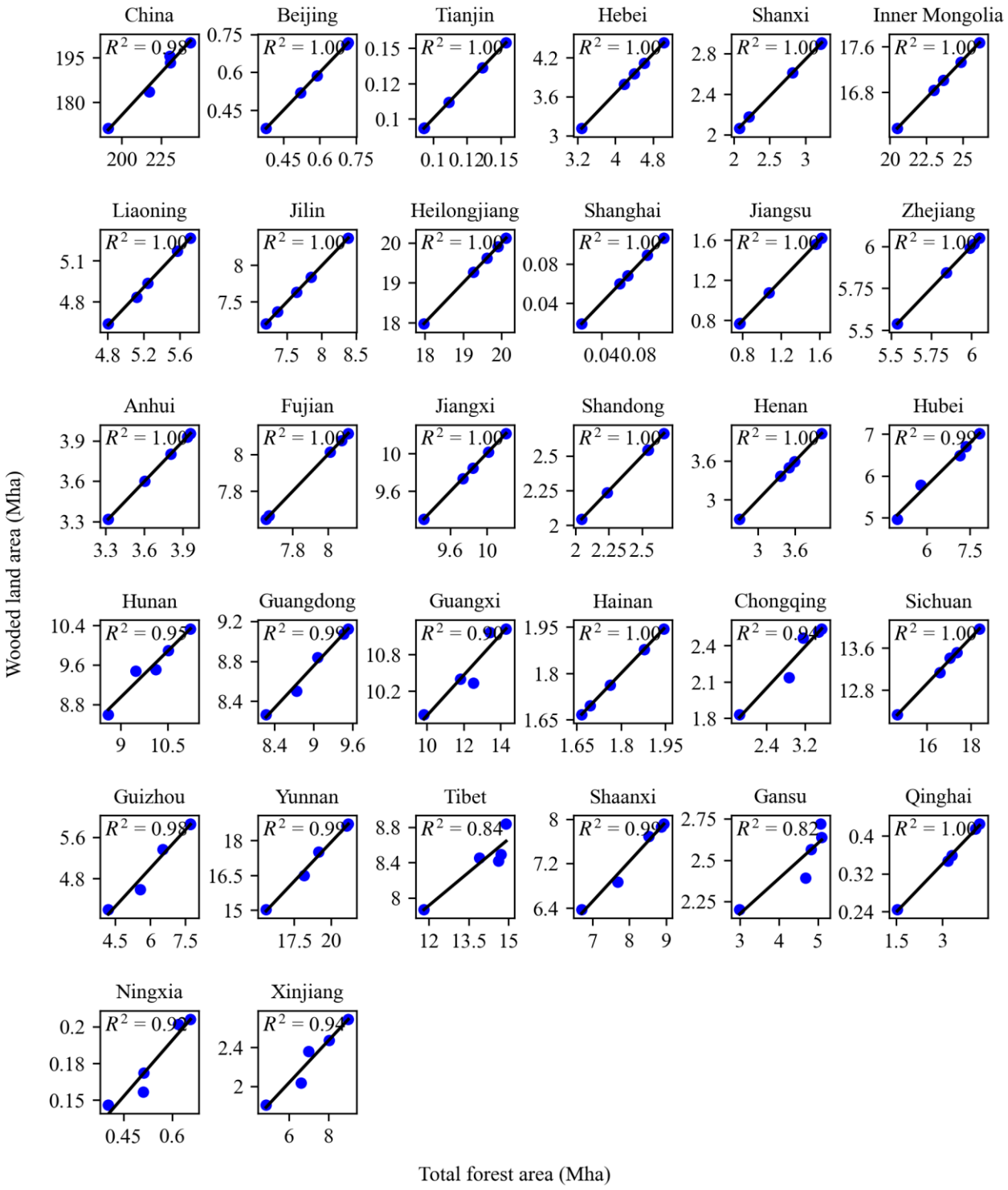

15 **Figure S3.** Extrapolation of wooded land area for each province in China.

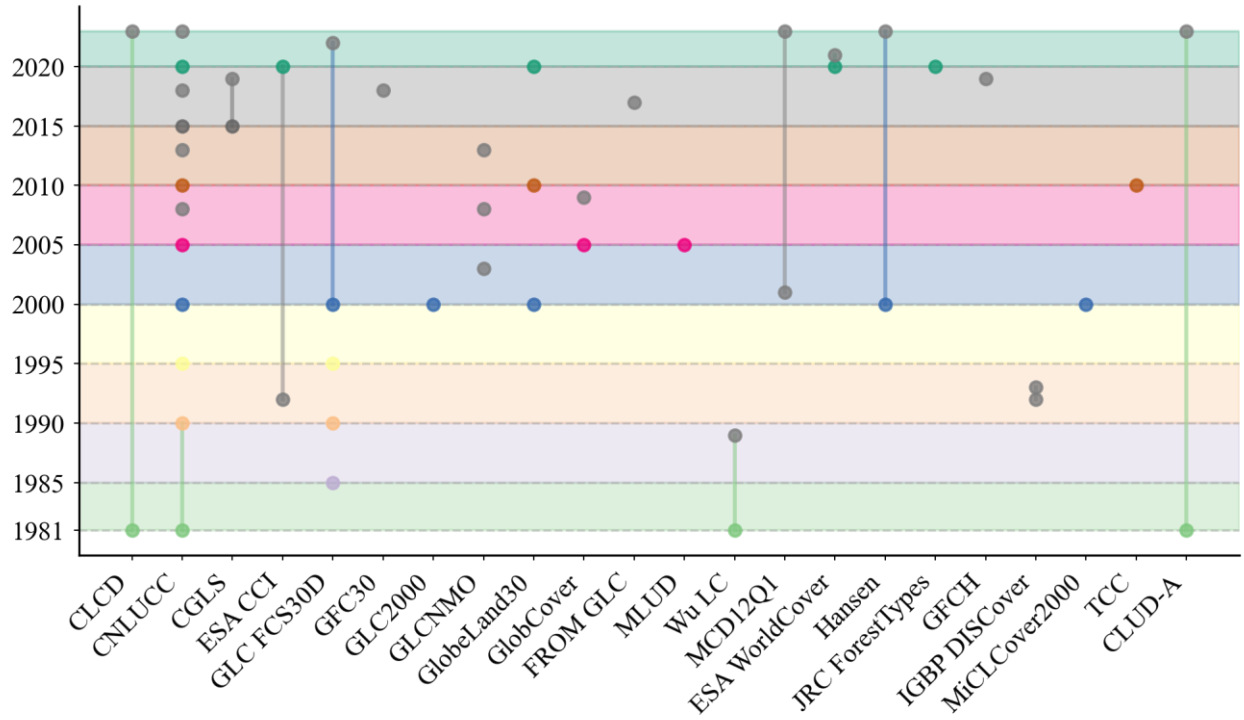

Figure S4. Schematic diagram of the temporal coverage of land use and land cover (LULC) products for forest reconstruction.

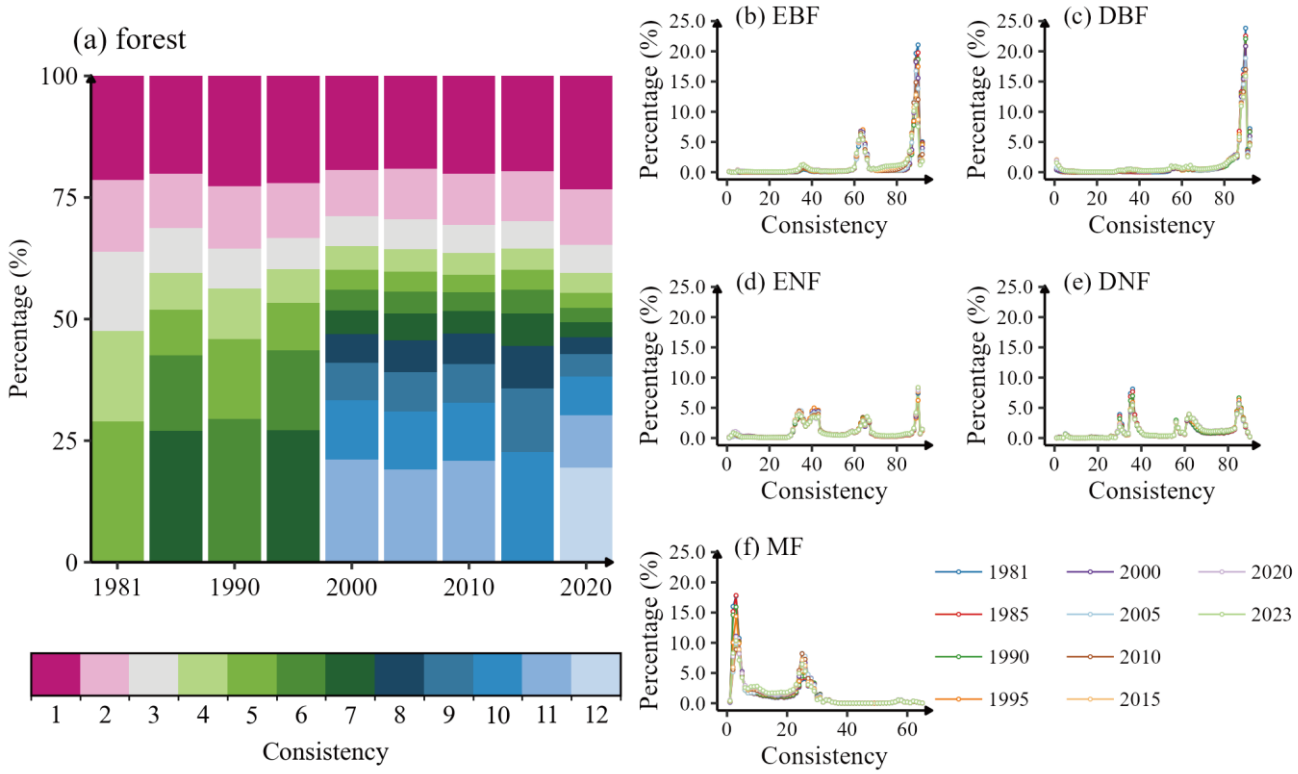

Figure S5. Inter-dataset consistency of forest cover in China. **(a)** Proportional distribution of potential forest pixels in China by consistency level for the years 1981, 1985, 1990, 1995, 2000, 2005, 2010, 2015, and 2020. The potential forest mask was generated annually by aggregating pixels classified as "forest" across all available land use and land cover (LULC) datasets. Consistency (CON) is defined as the number of datasets classifying a given pixel as forest; higher CON values therefore indicate greater inter-dataset agreement and a higher probability of a true forest classification. **(b–f)** Distribution of cross-dataset consistency scores for the five reconstructed plant functional types (PFTs) for the period 1981–2023: **(b)** evergreen broadleaf forests (EBF), **(c)** deciduous broadleaf forests (DBF), **(d)** evergreen needleleaf forests (ENF), **(e)** deciduous needleleaf forests (DNF), and **(f)** mixed leaf forests (MF). These scores are derived from the PFT dataset reconstructed in this study, where higher scores signify greater confidence in the PFT classifications.

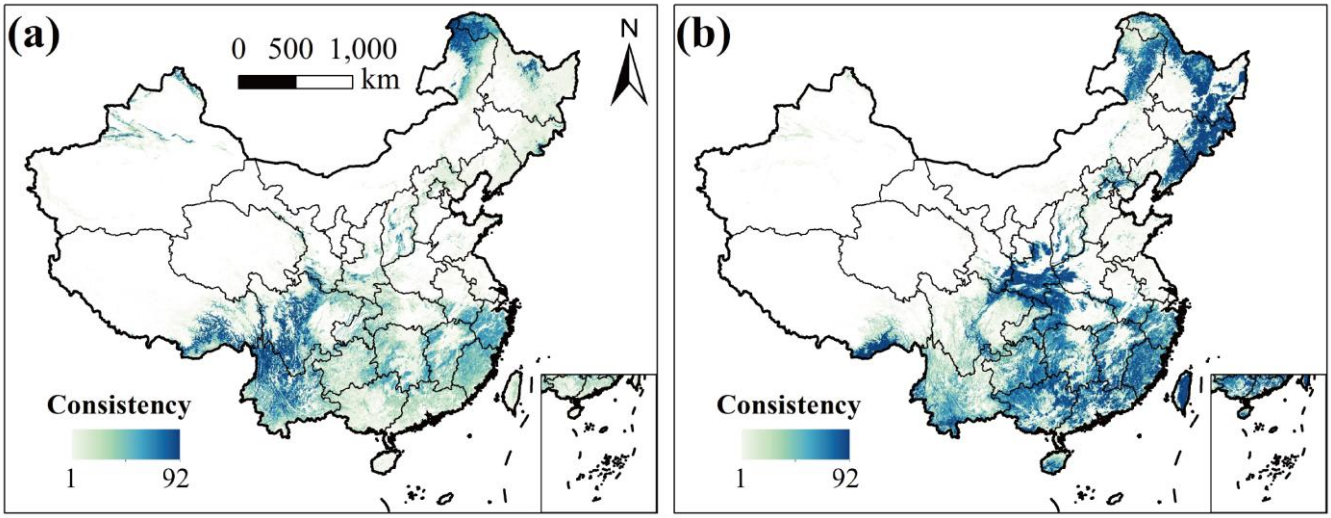

Figure S6. Static consistency maps for **(a)** needleleaf forests and **(b)** broadleaf forests, generated using all available land use and land cover (LULC) products from the 1981–2023 period.

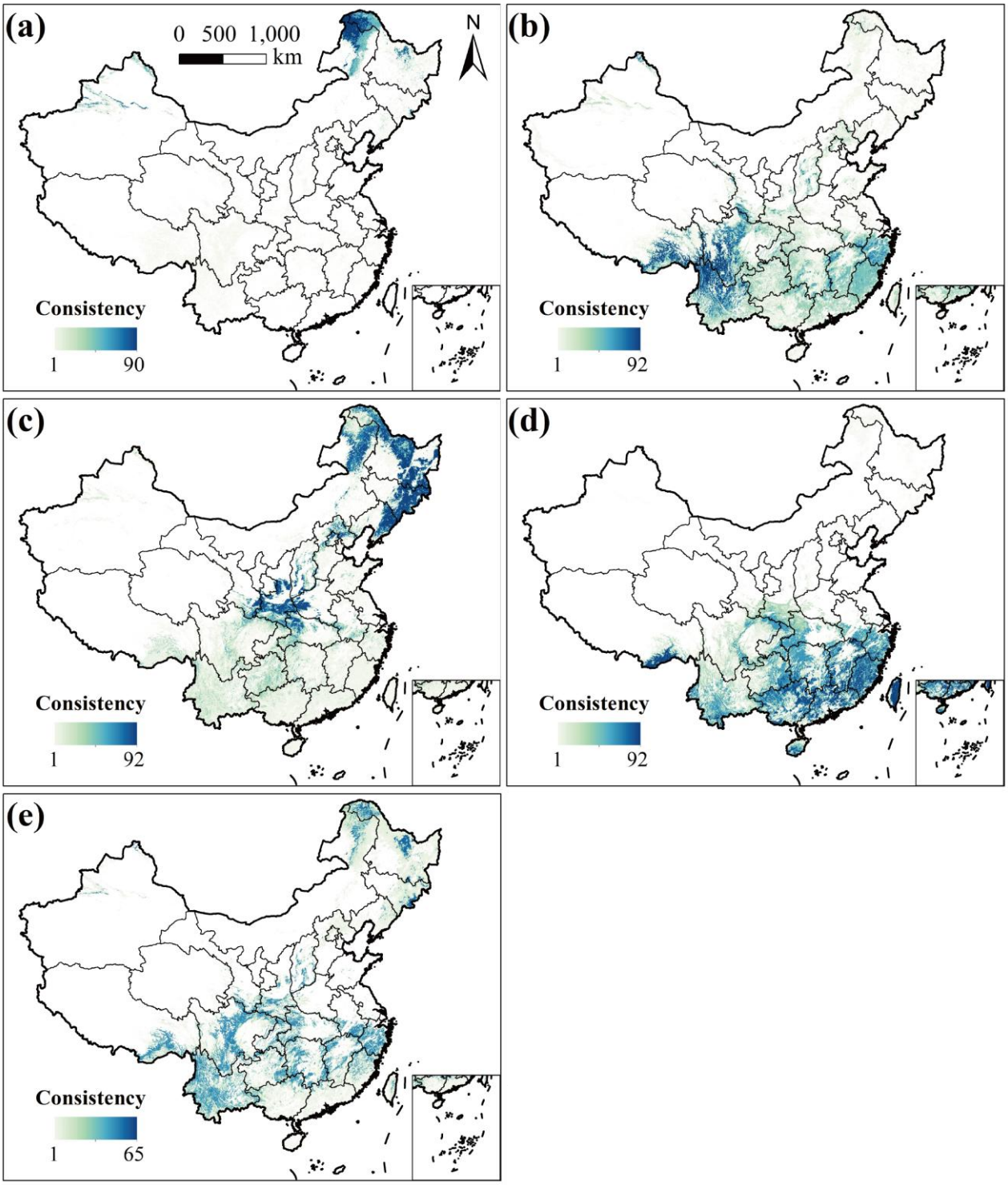

Figure S7. Static consistency maps for five subtypes, generated using all available data from the 1981–2023 period: **(a)** deciduous needleleaf, **(b)** evergreen needleleaf, **(c)** deciduous broadleaf, **(d)** evergreen broadleaf, and **(e)** mixed leaf forests.

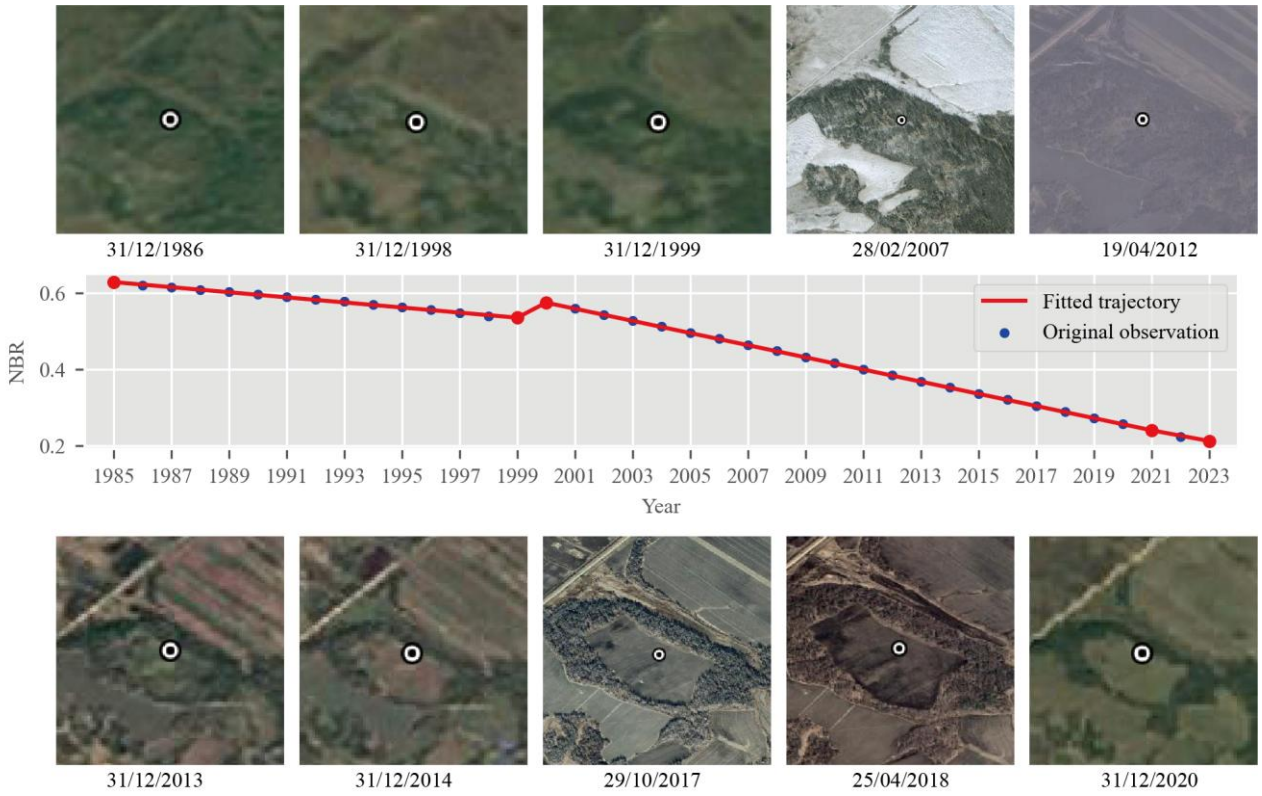

Figure S8. Time series example of an unstable plot (forest to nonforest transition). A forest loss event occurred in 2013. The historical Google Earth imagery time series illustrates the conversion process from forestland to nonforest. (Example location: 48.066463°N, 127.562063°E). In the time series plot, the horizontal axis represents the year, and the vertical axis denotes the normalized burn ratio (NBR). The blue points represent Landsat observations, the red lines denote the LandTrendr model fits, and the red dots indicate the vertices identified by the LandTrendr model. The concentric circles mark the location of the sample plot (Imagery © 2025 NASA, Map data © 2025 Google).

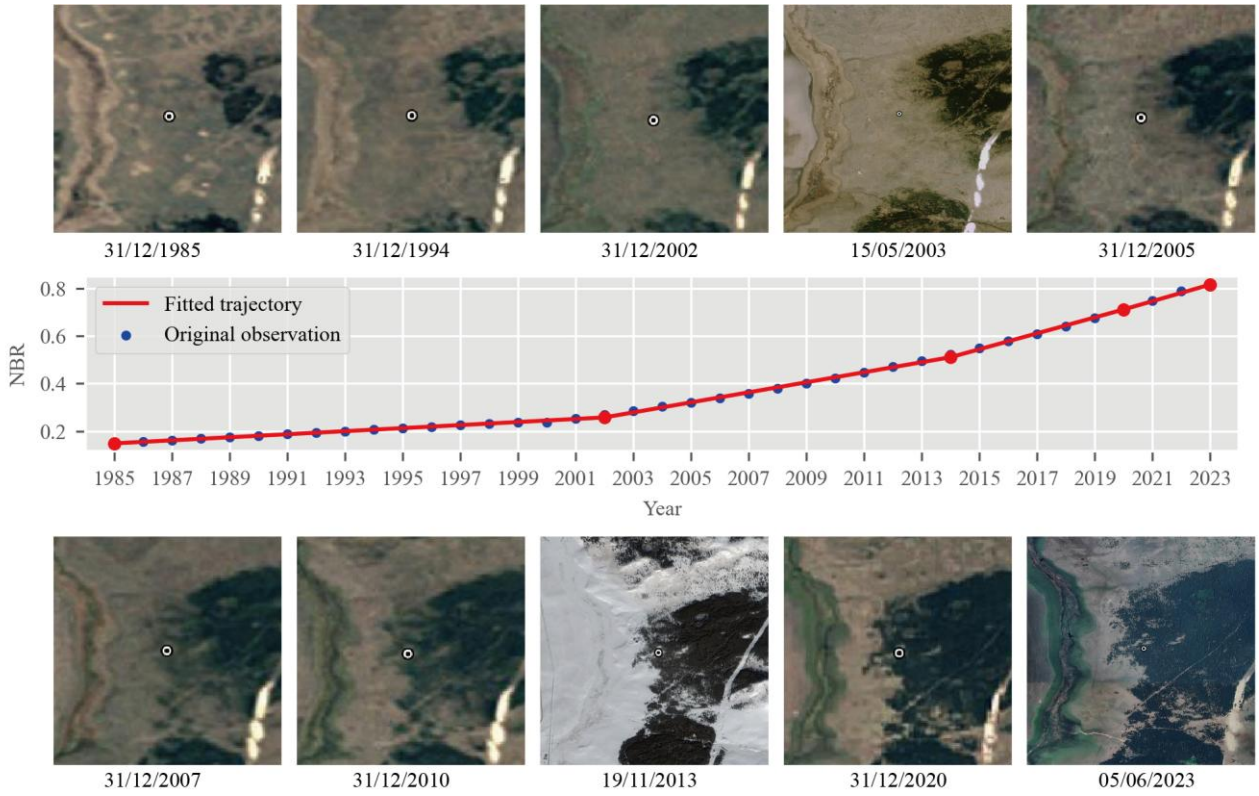

Figure S9. Time series example of an unstable plot (nonforest to forest transition). A forest gain event occurred in 2007. The historical Google Earth imagery time series illustrates the conversion process from nonforest to forest. (Example location: 47.857612°N, 119.494846°E). In the time series plot, the horizontal axis represents the year, and the vertical axis denotes the normalized burn ratio (NBR). The blue points represent Landsat observations, the red lines denote the LandTrendr model fits, and the red dots indicate the vertices identified by the LandTrendr model. The concentric circles mark the location of the sample plot (Imagery © 2025 NASA, Map data © 2025 Google).

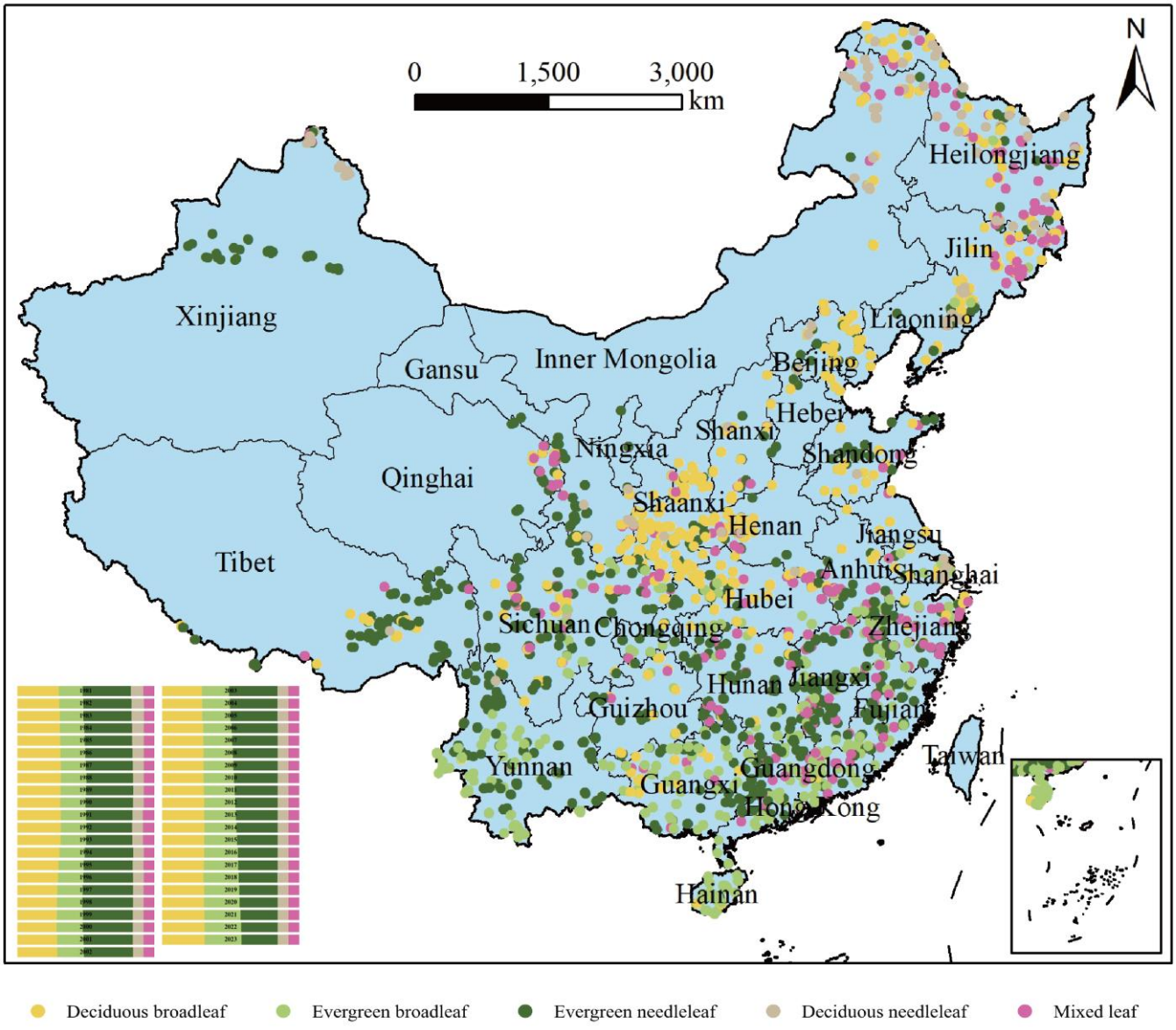

Figure S10. Spatial distribution of the independent forest validation sample points used for the accuracy assessment. The inset bar chart in the lower-left corner details the annual proportions of each land cover type.

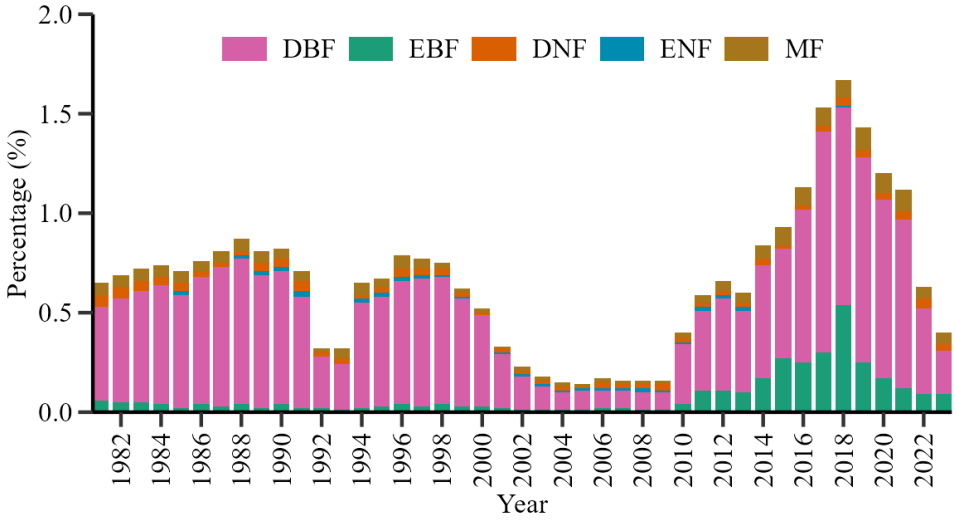

Figure S11. Percentage of pixels for the five reconstructed plant functional types (PFTs) not falling within their corresponding consistency type, 1981–2023. DBF: deciduous broadleaf forest, EBF: evergreen broadleaf forest, DNF: deciduous needleleaf forest, ENF: evergreen needleleaf forest, MF: mixed leaf forest.

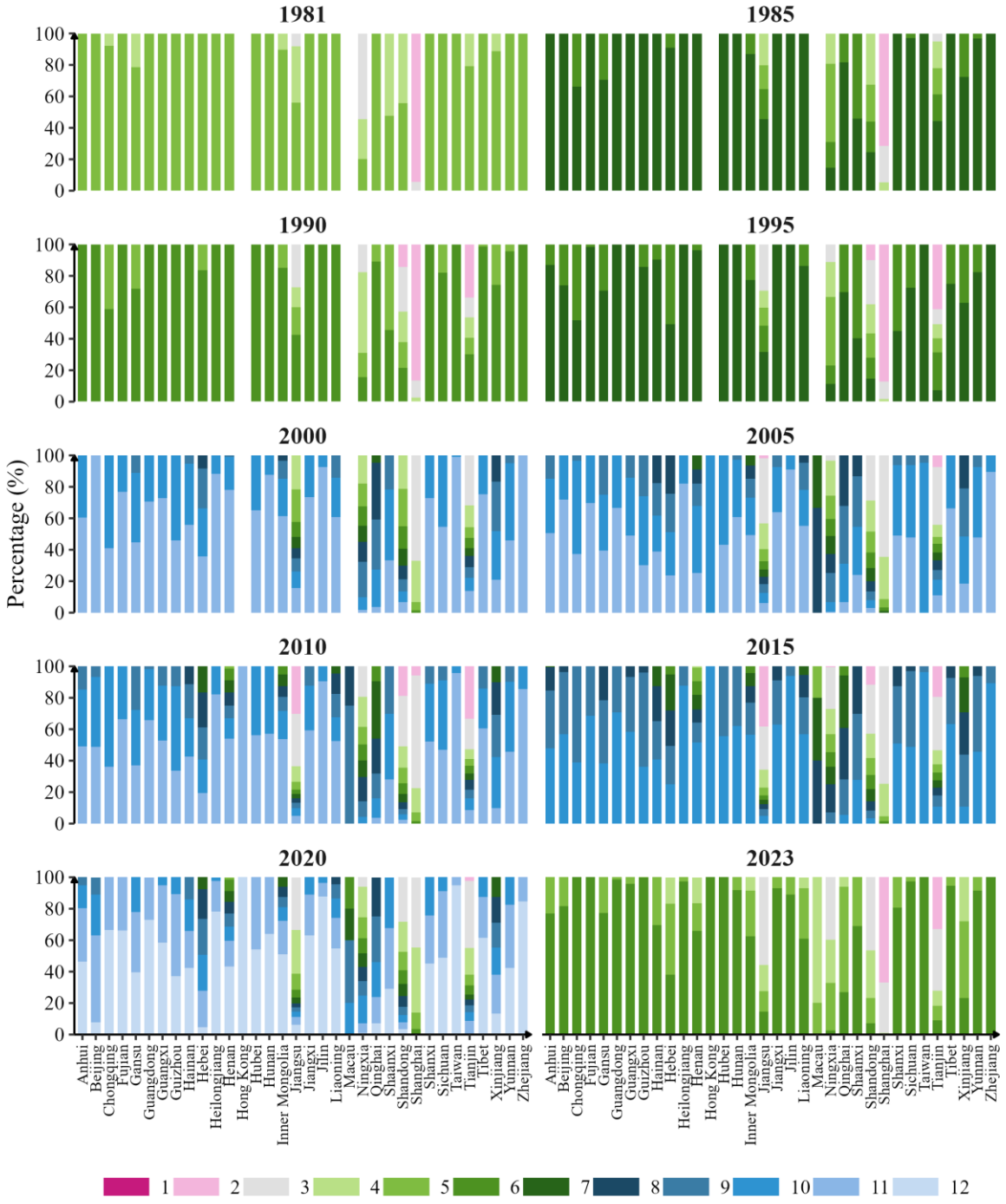

Figure S12. Provincial-level distribution of forest pixels according to their inter-dataset consistency score, assessed over the 1981–2023 period. Note: data for Hong Kong and Macau are unavailable for the 1981–2002 period, as their national forest inventories (NFI) were not implemented until after 2003.

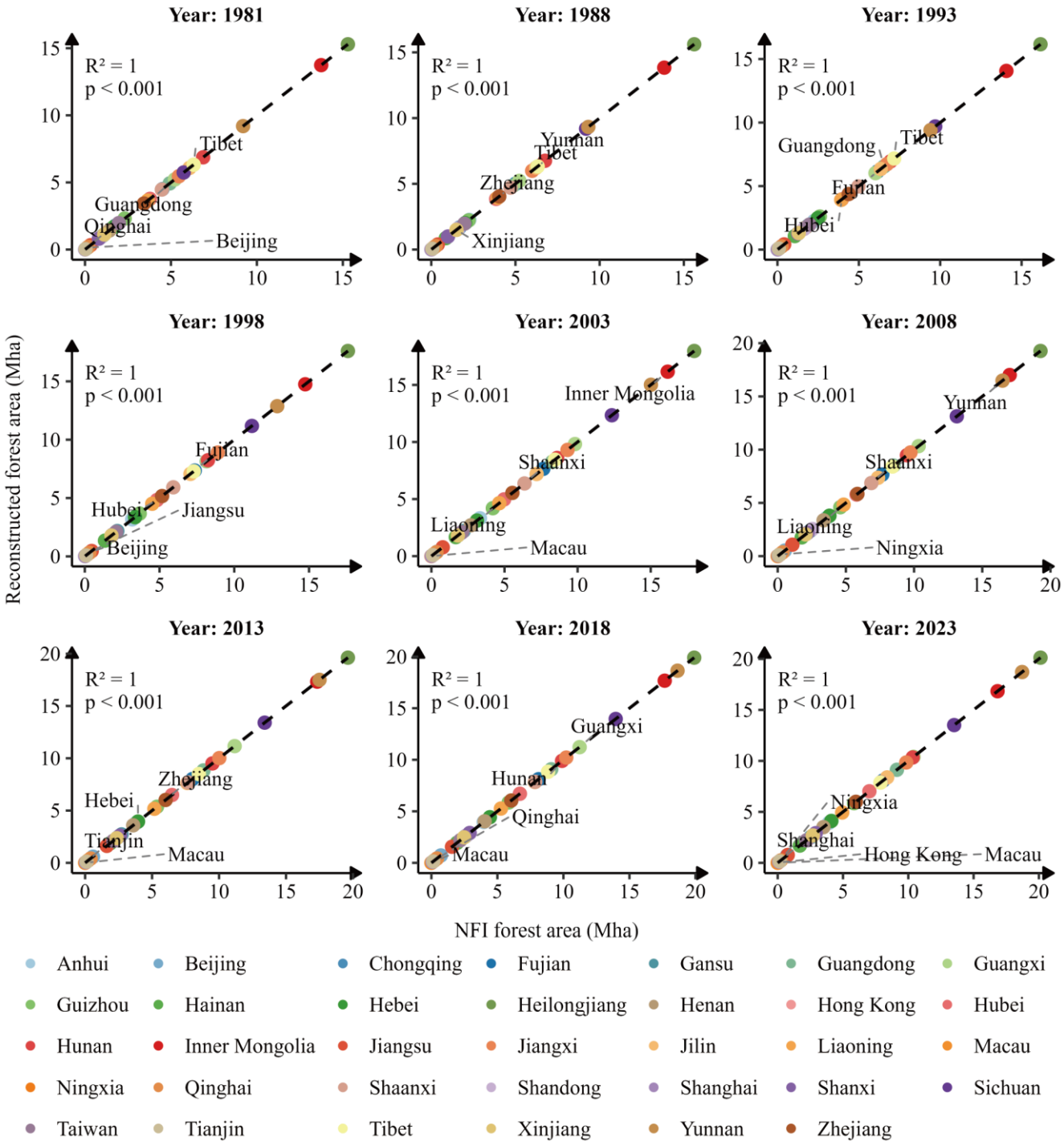

Figure S13. Scatter plot comparing provincial-level forest area as reported by the national forest inventory (NFI) with estimates from the reconstructed maps of this study.

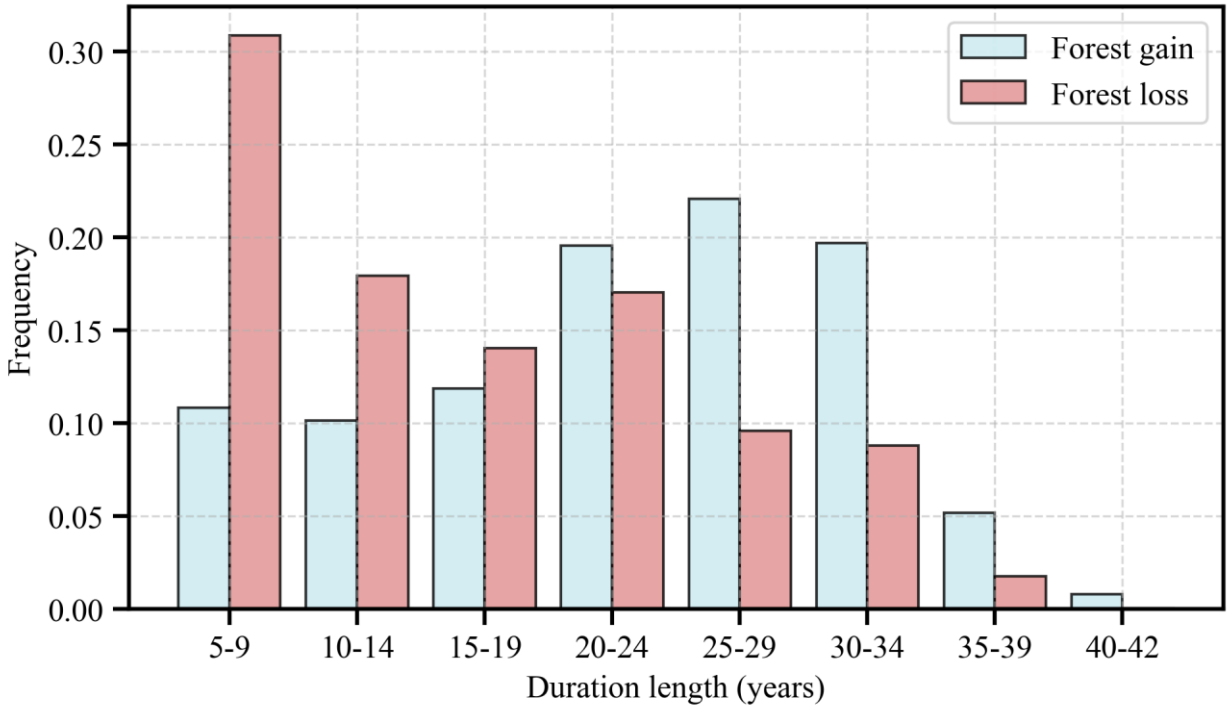

Figure S14. Frequency distribution histograms showing the duration of forest gain and loss events that occurred between 1981 and 2023.

Supplementary Tables S1 – S3

Table S1. Land use and land cover **(**LULC) datasets used in this study.

Datasets	Resolution	Time range	Data source
CLCD[a,c]	30 m	1980s–2023	(Yang and Huang, 2021)
CNLUCC[a]	30 m/1 km	1980s–2023	http://www.resdc.cn
CGLS[b,c]	100 m	2015–2019	(Buchhorn et al., 2020)
ESA_CCI[b,c]	300 m	1992–2020	https://data.ceda.ac.uk/neodc/esacci/land_cover/data
GLC_FCS30D[b,c]	30 m	1985–2022	(Zhang et al., 2024)
GFC30[a]	30 m	2018	(Zhang et al., 2020)
GLC2000[b]	1 km	2000	(Bartholomé and Belward, 2005)
GLCNMO[b]	1 km	2003, 2008, 2013	(Tateishi et al., 2011)
GlobeLand30[a]	30 m	2000, 2010, 2020	(Chen et al., 2015)
GlobCover[b]	300 m	2005, 2009	(Bontemps et al., 2011)
FROM_GLC[a]	10 m	2017	(Gong et al., 2019)
MLUD[a]	250 m	2005	(Ge et al., 2018)
Wu_LC[a]	1 km	1980s	http://www.resdc.cn
MCD12Q1[b,c]	500 m	2001–2023	(Sulla-Menashe et al., 2019)
ESA_WorldCover[a]	10 m	2020, 2021	https://esa-worldcover.org/en
Hansen[a,c]	30 m	2000–2023	(Hansen et al., 2013)
JRC_ForestTypes[a]	10 m	2020	(Bourgoin et al., 2025)
GFCH[a]	30 m	2019	(Potapov et al., 2021)
IGBP DISCover[b]	1 km	1992–1993	(Loveland et al., 1999)
MiCLCover[b]	1 km	2000	(Ran et al., 2009)
TCC[a]	30 m	2010	https://www.glad.geog.umd.edu/dataset/global-2010-tree-cover-30-m
CLUD-A[a,c]	1 km	1981–2023	(Xu et al., 2020)

[a.] These datasets delineate a single, general forest category and lack classification into specific subtypes.

[b.] These datasets provide detailed classifications of various forest subtypes and were used for the plant functional types (PFTs) classification in this study.

[c.] These datasets are updated on an annual basis, in contrast to others which are produced only for specific years.

Table S2. Calibrated model parameters for each plant functional type (PFT). Respcoeff denotes the maintenance respiration coefficient for sustaining existing live tissue (e.g., enzyme replacement and ion balance); pstemp_low denotes the lower bound of the optimal temperature range for photosynthesis; pstemp_high denotes the upper bound of the optimal temperature range for photosynthesis; pstemp_min denotes the minimum temperature limit for photosynthesis; pstemp_max denotes the maximum temperature limit for photosynthesis; and lambda_max denotes the intrinsic water-use efficiency under non-water-limited conditions (i.e., stomata fully open). Values calibrated for this study are indicated in bold.

PFT name	Model parameters					
	respcoeff	pstemp_low (°C)	pstemp_high (°C)	pstemp_max (°C)	pstemp_min (°C)	lambda_max
Boreal evergreen needleleaf forest	1.0	10	25	38	-4	0.8 **(0.6)**
Deciduous needleleaf forest	1.0	10	25	38	-4	0.8 **(0.6)**
Temperate evergreen needleleaf forest	1.0 **(0.2)**	15 **(20)**	25 **(30)**	38 **(42)**	-2 **(2)**	0.8 **(0.6)**
Temperate deciduous broadleaf forest	1.0	15	25	38	-2	0.8 **(0.6)**
Boreal deciduous broadleaf forest	1.0	10	25	38	-4	0.8 **(0.6)**
Temperate evergreen broadleaf forest	1.0 **(0.2)**	15 **(20)**	25 **(30)**	38 **(42)**	-2 **(2)**	0.8 **(0.6)**
Tropical evergreen broadleaf forest	0.15	25	30	55	2	0.8 **(0.6)**
Tropical deciduous broadleaf forest	0.15	25	30	55	2	0.8 **(0.6)**

Table S3. Proportion of changed area between needleleaf and broadleaf forests relative to the ending year across different datasets, assessed over five-year intervals.

Datasets	Period	Mutual conversion between needleleaf and broadleaf forests (Mha)	Total area of needleleaf and broadleaf forests at the end of the year (Mha)	Proportion of change
GLC_FCS30D	1985–1990	0.3975	237.41	0.17%
ESA CCI	1995–2000	0	168.89	0.00%
MCD12Q1	2005–2010	0.2175	63.84	0.34%

References

Bartholomé, E., and Belward, A. S.: GLC2000: a new approach to global land cover mapping from Earth observation data, *Int. J. Remote Sens.*, 26, 1959–1977, https://doi.org/10.1080/01431160412331291297, 2005.

Bontemps, S., Defourny, P., Van Bogaert, E., Arino, O., Kalogirou, V., and Perez, J. J. R.: GLOBCOVER 2009 Products description and validation report, ESA, 2011.

Bourgoin, C., Verhegghen, A., Carboni, S., Degreve, L., Ameztoy Aramendi, I., Ceccherini, G., Colditz, R., and Achard, F.: Global forest maps for the year 2020 to support the EU regulation on deforestation-free supply chains, Publications Office of the European Union, Luxembourg, https://data.europa.eu/doi/10.2760/1975879, 2025.

Buchhorn, M., Lesiv, M., Tsendbazar, N.-E., Herold, M., Bertels, L., and Smets, B.: Copernicus global land cover layers—collection 2, *Remote Sens.*, 12, 1044, https://doi.org/10.3390/rs12061044, 2020.

Chen, J., Chen, J., Liao, A., Cao, X., Chen, L., Chen, X., He, C., Han, G., Peng, S., and Lu, M.: Global land cover mapping at 30 m resolution: A POK-based operational approach, *ISPRS J. Photogramm. Remote Sens.*, 103, 7–27, https://doi.org/10.1016/j.isprsjprs.2014.09.002, 2015.

Ge, Y., Jia, Y., Chen, Y., Xu, X., Jiang, D., and Zhang, D.: A multi-scale provincial land use dataset of the Chinese mainland based on super-resolution mapping, *J. Glob. Change Data Discov.*, 2, 323–330, https://doi.org/10.3974/geodp.2018.03.11, 2018.

Gong, P., Liu, H., Zhang, M., Li, C., Wang, J., Huang, H., Clinton, N., Ji, L., Li, W., Bai, Y., Chen, B., Xu, B., Zhu, Z., Yuan, C., Su, H. P., Guo, J., Xu, N., Li, W., Zhao, Y., Yang, J., Yu, C., Wang, X., Fu, H., Li, X., Li, W., Liu, C., Xu, F., Zhang, H., Chen, J., Feng, X., and Zhang, H.: Stable classification with limited sample: Transferring a 30-m resolution sample set collected in 2015 to mapping 10-m resolution global land cover in 2017, *Sci. Bull.*, 64, 370–373, https://doi.org/10.1016/j.scib.2019.03.002, 2019.

Hansen, M. C., Potapov, P. V., Moore, R., Hancher, M., Turubanova, S. A., Tyukavina, A., Thau, D., Stehman, S. V., Goetz, S. J., Loveland, T. R., Kommareddy, A., Egorov, A., Chini, L., Justice, C. O., and Townshend, J. R. G.: High-resolution global maps of 21st-century forest cover change, *Science*, 342, 850–853, https://doi.org/10.1126/science.1244693, 2013.

Loveland, T. R., Zhu, Z., Ohlen, D. O., Brown, J. F., Reed, B. C., and Yang, L.: An analysis of the IGBP global land-cover characterization process, *Photogramm. Eng. Remote Sens*., 65, 1021–1032, 1999.

Potapov, P., Li, X., Hernandez-Serna, A., Tyukavina, A., Hansen, M. C., Kommareddy, A., Pickens, A., Turubanova, S., Tang, H., Silva, C. E., Armston, J., Dubayah, R., Blair, J. B., and Hofton, M.: Mapping global forest canopy height through integration of GEDI and Landsat data, *Remote Sens. Environ.*, 253, 112165, https://doi.org/10.1016/j.rse.2020.112165, 2021.

Ran, Y., Lu, L., and Li, X.: China Land Cover Classification at 1 km Spatial Resolution Based on a Multi-source Data Fusion Approach, *Adv. Earth Sci*., 24, 192–203, http://www.adearth.ac.cn/CN/10.11867/j.issn.1001-8166.2009.02.0192, 2009.

Sulla-Menashe, D., Gray, J. M., Abercrombie, S. P., and Friedl, M. A.: Hierarchical mapping of annual global land cover 2001 to present: The MODIS Collection 6 Land Cover product, *Remote Sens. Environ.*, 222, 183–194, https://doi.org/10.1016/j.rse.2018.12.013, 2019.

Tateishi, R., Uriyangqai, B., Al-Bilbisi, H., Ghar, M. A., Tsend-Ayush, J., Kobayashi, T., Kasimu, A., Hoan, N. T., Shalaby, A., Alsaaideh, B., Enkhzaya, T., Gegentana, and Sato, H. P.: Production of global land cover data–GLCNMO, *Int. J. Digit. Earth*, 4, 22–49, https://doi.org/10.1080/17538941003777521, 2011.

Xu, Y., Yu, L., Peng, D., Zhao, J., Cheng, Y., Liu, X., Li, W., Meng, R., Xu, X., and Gong, P.: Annual 30-m land use/land cover maps of China for 1980–2015 from the integration of AVHRR, MODIS and Landsat data using the BFAST algorithm, *Sci. China Earth Sci*., 63, 1390–1407, https://doi.org/10.1007/s11430-019-9606-4, 2020.

Yang, J. and Huang, X.: The 30 m annual land cover dataset and its dynamics in China from 1990 to 2019, *Earth Syst. Sci. Data*, 13, 3907–3925, https://doi.org/10.5194/essd-13-3907-2021, 2021.

Zhang, X., Long, T., He, G., Guo, Y., Yin, R., Zhang, Z., Xiao, H., Li, M., and Cheng, B.: Rapid generation of global forest cover map using Landsat based on the forest ecological zones, *J. Appl. Remote Sens.*, 14, 022211, https://doi.org/10.1117/1.JRS.14.022211, 2020.

Zhang, X., Zhao, T., Xu, H., Liu, W., Wang, J., Chen, X., and Liu, L.: GLC_FCS30D: the first global 30 m land-cover dynamics monitoring product with a fine classification system for the period from 1985 to 2022 generated using dense-time-series Landsat imagery and the continuous change-detection method, *Earth Syst. Sci. Data*, 16, 1353–1381, https://doi.org/10.5194/essd-16-1353-2024, 2024.